IEEE Robotics and Automation Letters (RA-L) paper, presented at ICRA 2024, Yokohama, Japan. Cite as RA-L paper.

The Kinematics of Constant Curvature Continuum Robots Through Three Segments

Yucheng Li, David H. Myszka, and Andrew P. Murray

***Abstract*—This letter investigates the mathematical relationships between the positions and orientations at the segment tips of a piecewise constant curvature (PCC) continuum robot with up to three segments. For one-segment, a reachability criterion is proposed, simplifying the calculation of the neighboring orientation. For two-segments, a reachability criterion is proposed and the redundancy of its inverse kinematics solution is found, establishing a circle of tip locations. For three-segments, the redundancy of the inverse kinematics includes tips that lie on a sphere providing a closed-form solution to the inverse kinematics problem. These relationships are derived from the unique characteristics of the bisecting plane of a single segment. The degenerate cases for the solutions are also addressed. These outcomes stem from a specific PCC parametrization, with implications extending to the general PCC model. Note that this study is grounded solely in simulation.**

***Index Terms*—Kinematics, formal methods in robotics and automation, soft robot applications, constant curvature, continuum robots.**

I. Introduction

THE concept of continuum robots is inspired by biological organisms including snakes, octopus tentacles, and elephant trunks to emulate their impressive flexibility and shape-changing abilities [1]. With infinite degrees of freedom (DoF), continuum robots are capable of adapting to various environments and navigating within constrained spaces [2]. Continuum robots show promise in medical [3] and industrial applications [4]. Research investigations include both experimental [5] and theoretical pursuits [6], [7].

The mathematical modeling of a continuum robot includes its kinematics, force distribution, and material mechanics, effectively capturing its motion and physical characteristics [8]. The *backbone* of a continuum robot is a continuous spatial curve that characterizes the robot's shape and its spatial positioning [9]. Various models can represent the backbone's shape including variable curvature kinematic models [10], modal techniques [11], and piecewise kinematics approaches [12]. Although discrete models of continuum robots are known to be less accurate than continuous models due to the influence of external and body loads, friction, and other factors, they still have advantages [13]. One such advantage is their ability to approximate robot kinematics using diverse elements, including pseudo-rigid bodies [12], the absolute nodal coordinates [14], and the piecewise constant strain [15]. Using discrete elements facilitates the integration of rigid-body techniques in modeling the nonlinear behavior of continuum robots and analyzing their dynamics. The piecewise constant curvature (PCC) model represents a continuum robot as a sequence of PCC elements, where all states except for bending are set to zero and is a special case of the piecewise constant strain model [16], [17]. Continuum robots in use demonstrate deviations from the PCC model [8] especially under significant external forces [14]. Yet, the PCC model provides a close approximation to the shape of several in-use continuum and soft robot designs including the PneuNet [18] and FREE [19]. As such, geometric insights and inverse kinematic solutions can be directly applied to the design and control of such robots. Direct and quantitative comparisons of the accuracy of the PCC model are in [20].

The kinematics of continuum robots involves two key mappings: the mapping that relates the joint variables to the configuration parameters [21], and the mapping that relates the configuration parameters to the end-effector pose [1]. Many researchers use the PCC model for kinematic mappings, including Neppalli et al. [22], Xu and Simaan [23], and Zhao et al. [24]. Despite the existence of numerous studies on the kinematics of continuum robots in the literature [1], [8], the analysis of reachability and redundancy in the inverse kinematics remains an unresolved issue [13], [25].

Although Jacobian-based solutions to the inverse kinematics are widely implemented [26], [27], [28], they have significant computational time depending on the end-effector pose, and singularity issues, especially when redundancies exist. Furthermore, these approaches do not offer sufficient insight into the kinematics, leading to path planning and control complications. Lu et al. [29] proposed a computationally efficient inverse kinematics numerical method for an inextensible continuum robot utilizing the Kepler oval. Wang et al. [7] numerically solved the inverse kinematics of one or two inextensible segments with a one-dimensional nonlinear equation. Some inverse kinematics approaches use a spatial curve to approximate the robot's entire backbone [30], [31], [32].

Closed-form solutions to the inverse kinematics problem for two-segment continuum robots are achieved by utilizing quaternions [6]. That research includes identifying the intermediate tip's location, situated along an elliptical curve on a plane.

Manuscript received 20 June 2023; accepted 18 September 18 2023. Date of publication 29 September 2023; date of current version 1 March 2024. This letter was recommended for publication by Associate Editor J. Hughes and Editor Y.-L. Park upon evaluation of the reviewers' comments. This work was supported by the University of Dayton Office for Graduate Academic Affairs through the Graduate Student Summer Fellowship Program. *(Corresponding author: Yucheng Li.)*

The authors are with the Design of Innovative Machines Laboratory (DIMLab), Department of Mechanical and Aerospace Engineering, University of Dayton, Dayton, OH 45469, USA (e-mail: liy054@udayton.edu; dmyszka@udayton.edu; murray@udayton.edu).

This letter has supplementary downloadable material available at https://doi.org/10.1109/LRA.2023.3320946, provided by the authors.

Digital Object Identifier 10.1109/LRA.2023.3320946

IEEE Robotics and Automation Letters (RA-L) paper, presented at ICRA 2024, Yokohama, Japan. Cite as RA-L paper.

IEEE Robotics and Automation Letters (RA-L) paper, presented at ICRA 2024, Yokohama, Japan. Cite as RA-L paper.

Additionally, the work notes that a three-segment continuum robot can achieve the six-DoF at the end-effector, resulting in three-DoF redundancy in the solutions.

This letter proposes closed-form, simulation-based, solutions to the inverse kinematics of continuum robots with up to three segments, along with reachability criteria of one- and two-segment continuum robots that address degenerate cases in the solutions. To gain geometric insight into the inverse kinematics of continuum robots, this letter conducts a redundancy analysis that leads to the identification of the tip circle and tip sphere as the closed-form solutions to the inverse kinematics problems of two- and three-segment continuum robots, respectively. These geometric findings are obtained by analyzing the features of the bisecting plane of a one-segment continuum robot, which provides a comprehensive explanation of the strongly coupled relationship between the position and orientation at the end-effector. An important distinction is that the analysis in this letter focuses on tip positions and orientations without relying on joint variables, while prior works in [1] and [21] focus on joint variables and their mathematical relationships.

The remainder of the letter is organized as follows: Sec. II provides an overview of the mapping between the configuration parameters and the tip poses of PCC continuum robots. Section III introduces the bisecting plane, the reachability criterion of one-segment continuum robots, and the simplified calculation between the neighboring orientations. Section IV proposes the reachability criterion of two-segment continuum robots, investigates the kinematic redundancy in the inverse kinematics problem of two-segment continuum robots, and introduces the tip circle. Section V investigates the kinematic redundancy in the inverse kinematics problem of three-segment continuum robots, and introduces the tip sphere. Section VI discusses the degenerate cases in the inverse kinematics of two- and three-segment continuum robots. Lastly, Sec. VII concludes the letter.

II. Background: PCC Forward Kinematics

In the PCC model, a continuum robot is characterized by a spatial curve that is constructed using a sequence of circular arcs, which are tangentially connected and aligned end-to-end. This spatial curve is commonly referred to as the backbone of the continuum robot, where each circular arc corresponds to a distinct segment of the robot. The points of tangential alignment between neighboring segments are denoted as tips.

This letter utilizes the notation $\boldsymbol{d}_i^j \in \mathbb{R}^3$ to denote the vector from tip j to tip i and $\boldsymbol{R}_i^j \in \boldsymbol{SO}(3)$ for the rotation matrix between their corresponding orientations relative to frame j. Without loss of generality, it is assumed that the base position of the continuum robot is situated at the origin, while the base orientation is represented by the identity matrix $\boldsymbol{I}^{3\times3}$. To simplify the notation, a single subscript $\boldsymbol{d}_i$ is utilized instead of $\boldsymbol{d}_i^0$ to denote the distance between the base and tip i. Similarly, the rotation matrix between the orientations of the base and tip i is represented by $\boldsymbol{R}_i$, as illustrated in Fig. 1.

The specification of a segment in the configuration space relies on three parameters: the bending angle $\theta_i \in [0, 2\pi)$, the azimuth angle $\phi_i \in (-\pi, \pi]$, and the segment arc length

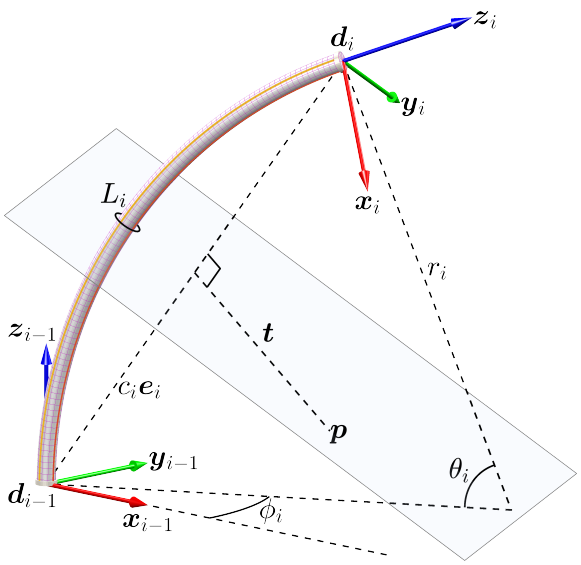

Fig. 1. A schematic of one bent segment of a continuum robot. The point $\boldsymbol{p}$ may be arbitrarily selected on the bisecting plane.

$L_i \in \mathbb{R}^+$. The mapping from the three configuration parameters to the segment tip pose is represented by the transformation $\boldsymbol{T}_i^{i-1} \in \boldsymbol{SE}(3)$,

$$\boldsymbol{T}_i^{i-1} = \begin{bmatrix} \boldsymbol{R}_i^{i-1} & \boldsymbol{d}_i^{i-1} \\ \boldsymbol{0}^\intercal & 1 \end{bmatrix}, \tag{1}$$

where the rotation matrix is

$$\boldsymbol{R}_i^{i-1} = \boldsymbol{Z}(\phi_i)\boldsymbol{Y}(\theta_i)\boldsymbol{Z}(-\phi_i), \tag{2}$$

where $\boldsymbol{Z}$ and $\boldsymbol{Y}$ are intrinsic rotations around the $\{0,0,1\}^\intercal$ and $\{0,1,0\}^\intercal$ axes, respectively. Expanding $\boldsymbol{R}_i^{i-1}$ reveals that the three columns correspond to the $\boldsymbol{x}$-, $\boldsymbol{y}$-, and $\boldsymbol{z}$-axes of frame i in the local reference frame $i-1$,

$$\boldsymbol{x}_i^{i-1} = \begin{Bmatrix} \cos^2\phi_i(\cos\theta_i - 1) + 1 \\ \sin\phi_i\cos\phi_i(\cos\theta_i - 1) \\ -\cos\phi_i\sin\theta_i \end{Bmatrix}, \tag{3}$$

$$\boldsymbol{y}_i^{i-1} = \begin{Bmatrix} \sin\phi_i\cos\phi_i(\cos\theta_i - 1) \\ \sin^2\phi_i(\cos\theta_i - 1) + 1 \\ -\sin\phi_i\sin\theta_i \end{Bmatrix}, \tag{4}$$

$$\boldsymbol{z}_i^{i-1} = \begin{Bmatrix} \cos\phi_i\sin\theta_i \\ \sin\phi_i\sin\theta_i \\ \cos\theta_i \end{Bmatrix}. \tag{5}$$

The transformation in Eq. (1) relates the neighboring tip frames $i-1$ and i, enabling the successive calculation of the orientation of tip i in the fixed frame,

$$\boldsymbol{R}_i = \boldsymbol{R}_{i-1}\boldsymbol{R}_i^{i-1}. \tag{6}$$

The distance between tips $i-1$ and i in the local reference frame $i-1$ is

$$\boldsymbol{d}_i^{i-1} = r_i \begin{Bmatrix} \cos\phi_i(1 - \cos\theta_i) \\ \sin\phi_i(1 - \cos\theta_i) \\ \sin\theta_i \end{Bmatrix}, \tag{7}$$

where $r_i = L_i/\theta_i$ is the bending radius of the segment. When the bending angle $\theta_i = 0$, the translation vector is observed to

IEEE Robotics and Automation Letters (RA-L) paper, presented at ICRA 2024, Yokohama, Japan. Cite as RA-L paper.

be $\boldsymbol{d}_i^{i-1} = \{0, 0, L_i\}^\intercal$. Similar to Eq. (6), the position of tip i in the fixed frame is

$$\boldsymbol{d}_i = \boldsymbol{d}_{i-1} + \boldsymbol{R}_{i-1}\boldsymbol{d}_i^{i-1}. \tag{8}$$

Thus, given the configuration parameters θ_i, ϕ_i, and L_i for $i = 1, \ldots, n$ segments of a continuum robot, Eqs. (2) to (8) can be used to calculate the tip poses relative to the fixed frame.

In the local reference frame, the distance between tips $i-1$ and i can be written as the magnitude of the distance c_i multiplied by the unit vector between the tips $\boldsymbol{e}_i^{i-1}$,

$$\boldsymbol{d}_i^{i-1} = c_i \boldsymbol{e}_i^{i-1}, \tag{9}$$

where,

$$c_i = \left\|\boldsymbol{d}_i^{i-1}\right\| = \begin{cases} 2r_i \sin\frac{\theta_i}{2}, & \theta_i \neq 0, \\ L_i, & \theta_i = 0, \end{cases} \tag{10}$$

and,

$$\boldsymbol{e}_i^{i-1} = \frac{\boldsymbol{d}_i^{i-1}}{\left\|\boldsymbol{d}_i^{i-1}\right\|} = \begin{Bmatrix} \sin\frac{\theta_i}{2}\cos\phi_i \\ \sin\frac{\theta_i}{2}\sin\phi_i \\ \cos\frac{\theta_i}{2} \end{Bmatrix}. \tag{11}$$

The unit vector of segment i in the fixed frame is

$$\boldsymbol{e}_i = \boldsymbol{R}_{i-1}\boldsymbol{e}_i^{i-1} = \frac{\boldsymbol{d}_i - \boldsymbol{d}_{i-1}}{\left\|\boldsymbol{d}_i - \boldsymbol{d}_{i-1}\right\|}. \tag{12}$$

The three configuration parameters for each segment are calculated, in sequence from the base to the end-effector, with knowledge of the tip positions and the base frame. Equation (8) is first used to determine the tip's local position relative to its corresponding segment base. The bending and azimuth angles are then calculated with Eq. (11), and the segment length is determined using Eq. (10). This process extends to solving for the inverse kinematics problems of two- and three-segment continuum robots. In particular, the vector $\boldsymbol{e}_i$ proves useful throughout the subsequent derivations.

III. One-Segment Continuum Robot

This section presents the relationships for a single segment of a PCC continuum robot. The kinematic attributes of the segment are derived from the geometric properties of its bisecting plane, providing a foundation for subsequent sections in this letter. Specifically, the derivations of Eq. (33) in Sec. IV-A, Eqs. (39), (40), and (41) in Sec. IV-C, and Eq. (47) in Sec. V-A. In addition, the reachability of one-segment continuum robots is investigated, along with a simplified method for calculating orientations between neighboring frames relative to the fixed frame.

A. The Bisecting Plane

The bisecting plane of segment i is defined as the set of points equidistant from tips $i-1$ and i. This plane intersects the midpoint between the neighboring tips and is perpendicular to the vector $\boldsymbol{d}_i - \boldsymbol{d}_{i-1}$ connecting them. Selecting an arbitrary point $\boldsymbol{p}$ on the bisecting plane as shown in Fig. 1,

$$\boldsymbol{p} = \frac{\boldsymbol{d}_{i-1} + \boldsymbol{d}_i}{2} + \boldsymbol{t}, \tag{13}$$

where $\boldsymbol{t}$ is any vector such that

$$(\boldsymbol{d}_i - \boldsymbol{d}_{i-1}) \cdot \boldsymbol{t} = 0. \tag{14}$$

The bisecting plane has three properties. First, the angle between $\boldsymbol{x}_{i-1}$ and $\boldsymbol{d}_{i-1} - \boldsymbol{p}$ is equal to the angle between $\boldsymbol{x}_i$ and $\boldsymbol{d}_i - \boldsymbol{p}$,

$$\boldsymbol{x}_{i-1} \cdot (\boldsymbol{p} - \boldsymbol{d}_{i-1}) = \boldsymbol{x}_i \cdot (\boldsymbol{p} - \boldsymbol{d}_i). \tag{15}$$

Without loss of generality, Eq. (15) is shown by considering when $i - 1 = 0$. Substituting $\boldsymbol{d}_i^{i-1}$ (which is now $\boldsymbol{d}_1$) from Eq. (7) into Eq. (14) and letting $\boldsymbol{t} = \{t_0, t_1, t_2\}^\intercal$, where t_0 and t_1 are arbitrarily selected,

$$t_2 = \frac{\cos\theta_1 - 1}{\sin\theta_1}(t_0\cos\phi_1 + t_1\sin\phi_1). \tag{16}$$

Substituting $\boldsymbol{x}_i^{i-1}$ (which is now $\boldsymbol{x}_1$) from Eq. (3) and $\boldsymbol{p}$ from Eq. (13) into Eq. (15),

$$\begin{aligned} \boldsymbol{x}_0 \cdot (\boldsymbol{p} - \boldsymbol{d}_0) =& \boldsymbol{x}_1 \cdot (\boldsymbol{p} - \boldsymbol{d}_1) \\ =& \frac{L_1}{2\theta_1}\cos\phi_1(\cos\theta_1 - 1) - t_0, \end{aligned} \tag{17}$$

proving the relationship.

Second, the angle between $\boldsymbol{y}_{i-1}$ and $\boldsymbol{d}_{i-1} - \boldsymbol{p}$ is equivalent to the angle between $\boldsymbol{y}_i$ and $\boldsymbol{d}_i - \boldsymbol{p}$,

$$\boldsymbol{y}_{i-1} \cdot (\boldsymbol{p} - \boldsymbol{d}_{i-1}) = \boldsymbol{y}_i \cdot (\boldsymbol{p} - \boldsymbol{d}_i). \tag{18}$$

Third, the cosine of the angle between $\boldsymbol{z}_{i-1}$ and $\boldsymbol{d}_{i-1} - \boldsymbol{p}$ is the negative of the cosine of the angle between $\boldsymbol{z}_i$ and $\boldsymbol{d}_i - \boldsymbol{p}$, producing

$$\boldsymbol{z}_{i-1} \cdot (\boldsymbol{p} - \boldsymbol{d}_{i-1}) = -\boldsymbol{z}_i \cdot (\boldsymbol{p} - \boldsymbol{d}_i). \tag{19}$$

Note that the second and third properties are proven via a similar approach to the first property.

B. Reachability of One-Segment Continuum Robot

A criterion for the reachable position and orientation of a PCC continuum robot with a single segment can be identified. From Eq. (13), let $\boldsymbol{t} = \boldsymbol{0}$ such that $\boldsymbol{p}$ is the midpoint of the neighboring tips $i-1$ and i. Under this condition, Eqs. (15), (18), and (19) become

$$\begin{aligned} \boldsymbol{x}_{i-1} \cdot (\boldsymbol{d}_i - \boldsymbol{d}_{i-1}) =& -\boldsymbol{x}_i \cdot (\boldsymbol{d}_i - \boldsymbol{d}_{i-1}), \\ \boldsymbol{y}_{i-1} \cdot (\boldsymbol{d}_i - \boldsymbol{d}_{i-1}) =& -\boldsymbol{y}_i \cdot (\boldsymbol{d}_i - \boldsymbol{d}_{i-1}), \\ \boldsymbol{z}_{i-1} \cdot (\boldsymbol{d}_i - \boldsymbol{d}_{i-1}) =& \boldsymbol{z}_i \cdot (\boldsymbol{d}_i - \boldsymbol{d}_{i-1}). \end{aligned} \tag{20}$$

A segment being a circular arc has a corresponding chord that identifies the distance between neighboring tips. Equation (20) highlights the properties of this chord.

Considering the relationships in $\boldsymbol{x}$, adding one-half times the result of Eq. (20) to (15), and substituting Eq. (13),

$$\begin{aligned} (\boldsymbol{x}_i - \boldsymbol{x}_{i-1}) \cdot \boldsymbol{t} =& 0, \\ (\boldsymbol{y}_i - \boldsymbol{y}_{i-1}) \cdot \boldsymbol{t} =& 0, \\ (\boldsymbol{z}_i + \boldsymbol{z}_{i-1}) \cdot \boldsymbol{t} =& 0, \end{aligned} \tag{21}$$

where the $\boldsymbol{y}$ and $\boldsymbol{z}$ equations are generated similarly. Thus, $\boldsymbol{x}_i - \boldsymbol{x}_{i-1}$ is perpendicular to any value of $\boldsymbol{t}$ selected in the

IEEE Robotics and Automation Letters (RA-L) paper, presented at ICRA 2024, Yokohama, Japan. Cite as RA-L paper.

bisecting plane. As $\boldsymbol{t}$ is also perpendicular to the chord of segment i, $\boldsymbol{x}_i - \boldsymbol{x}_{i-1}$ and $\boldsymbol{d}_i - \boldsymbol{d}_{i-1}$ are parallel,

$$\boldsymbol{x}_i - \boldsymbol{x}_{i-1} \parallel \boldsymbol{d}_i - \boldsymbol{d}_{i-1}. \tag{22}$$

Likewise,

$$\boldsymbol{y}_i - \boldsymbol{y}_{i-1} \parallel \boldsymbol{d}_i - \boldsymbol{d}_{i-1}, \tag{23}$$

and,

$$\boldsymbol{z}_i + \boldsymbol{z}_{i-1} \parallel \boldsymbol{d}_i - \boldsymbol{d}_{i-1}. \tag{24}$$

The reachability criterion may now be explicitly stated. Let any two frames $\boldsymbol{R}_{i-1}$, $\boldsymbol{R}_i$, $\boldsymbol{d}_{i-1}$, and $\boldsymbol{d}_i$ be given. If Eqs. (22) to (24) are satisfied then these frames correspond to the neighboring frames of a one-segment continuum robot.

C. Orientation Calculation of Neighboring Frame

The rotation matrix relating neighboring frames may now be deduced from this reachability criterion. Let $\boldsymbol{R}_{i-1}$, $\boldsymbol{d}_{i-1}$, and $\boldsymbol{d}_i$, be given. The orientation $\boldsymbol{R}_i$ can be derived as follows.

From Eqs. (12) and (22) to (24),

$$\begin{aligned} \boldsymbol{e}_i &= \frac{\boldsymbol{d}_i - \boldsymbol{d}_{i-1}}{\|\boldsymbol{d}_i - \boldsymbol{d}_{i-1}\|} = \frac{\boldsymbol{x}_i - \boldsymbol{x}_{i-1}}{\|\boldsymbol{x}_i - \boldsymbol{x}_{i-1}\|} \\ &= \frac{\boldsymbol{y}_i - \boldsymbol{y}_{i-1}}{\|\boldsymbol{y}_i - \boldsymbol{y}_{i-1}\|} = \frac{\boldsymbol{z}_i + \boldsymbol{z}_{i-1}}{\|\boldsymbol{z}_i + \boldsymbol{z}_{i-1}\|}. \end{aligned} \tag{25}$$

Any one of these four statements may be used if one (or more) of them have a denominator of 0.

Substituting $\|\boldsymbol{x}_i - \boldsymbol{x}_{i-1}\| = \boldsymbol{e}_i^\mathsf{T}(\boldsymbol{x}_i - \boldsymbol{x}_{i-1})$ into Eq. (25),

$$\boldsymbol{e}_i \boldsymbol{e}_i^\mathsf{T}(\boldsymbol{x}_i - \boldsymbol{x}_{i-1}) = \boldsymbol{x}_i - \boldsymbol{x}_{i-1}. \tag{26}$$

Combining Eqs. (25) and (20),

$$\boldsymbol{e}_i \cdot \boldsymbol{x}_i = -\boldsymbol{e}_i \cdot \boldsymbol{x}_{i-1}. \tag{27}$$

Substituting Eq. (27) into (26), the $\boldsymbol{x}$-axis of frame i is

$$\boldsymbol{x}_i = (\boldsymbol{I} - 2\boldsymbol{e}_i \boldsymbol{e}_i^\mathsf{T})\boldsymbol{x}_{i-1}. \tag{28}$$

Via a similar approach, the $\boldsymbol{y}$- and $\boldsymbol{z}$-axes of frame i are found to be

$$\boldsymbol{y}_i = (\boldsymbol{I} - 2\boldsymbol{e}_i \boldsymbol{e}_i^\mathsf{T})\boldsymbol{y}_{i-1}, \tag{29}$$

and,

$$\boldsymbol{z}_i = -(\boldsymbol{I} - 2\boldsymbol{e}_i \boldsymbol{e}_i^\mathsf{T})\boldsymbol{z}_{i-1}. \tag{30}$$

Collecting Eqs. (28) to (30), the orientation of frame i is

$$\boldsymbol{R}_i = \left(\boldsymbol{I} - 2\boldsymbol{e}_i \boldsymbol{e}_i^T\right) \boldsymbol{R}_{i-1} \begin{bmatrix} 1 & 0 & 0 \\ 0 & 1 & 0 \\ 0 & 0 & -1 \end{bmatrix}. \tag{31}$$

Thus, given the position of both neighboring tips $i-1$ and i and the orientation of tip $i-1$, Eq. (31) determines the orientation of tip i eliminating the determination of the configuration parameters.

IV. Two-Segment Continuum Robot

This section presents the necessary conditions for a two-segment PCC continuum robot to attain a specified position and orientation at its end-effector. The general case is considered, where $\boldsymbol{R}_{i-1} \neq \boldsymbol{R}_{i+1}$ and $\boldsymbol{d}_{i-1} \neq \boldsymbol{d}_{i+1}$. Degenerate cases are discussed in Sec. VI. Additionally, the inverse kinematics problem of the two-segment continuum robot is investigated, offering geometric insight into the redundancy of the solutions.

A. Reachability of Two-Segment Continuum Robot

A criterion for the reachable position and orientation of a two-segment PCC continuum robot can be identified as the frames of two ends are related by six parameters. The plane determined by tips $i-1$, i, and $i+1$ is referred to as the *tip plane*. The normal vector to the tip plane may be readily determined. To simplify the notation, a single subscript $\boldsymbol{s}_i$ is utilized to denote the normal vector of the plane that intersects $\boldsymbol{d}_{i-1}$, $\boldsymbol{d}_i$, and $\boldsymbol{d}_{i+1}$. From the definition, $\boldsymbol{s}_i$ is perpendicular to the vector between both ends of the two-segment continuum robot,

$$(\boldsymbol{d}_{i+1} - \boldsymbol{d}_{i-1}) \cdot \boldsymbol{s}_i = 0. \tag{32}$$

Note that $\boldsymbol{s}_i$ has the same properties as the vector $\boldsymbol{t}$ from Eq. (14) for both segments i and $i+1$. From Eq. (21),

$$\begin{aligned} \boldsymbol{x}_{i-1} \cdot \boldsymbol{s}_i = \boldsymbol{x}_i \cdot \boldsymbol{s}_i = \boldsymbol{x}_{i+1} \cdot \boldsymbol{s}_i, \\ \boldsymbol{y}_{i-1} \cdot \boldsymbol{s}_i = \boldsymbol{y}_i \cdot \boldsymbol{s}_i = \boldsymbol{y}_{i+1} \cdot \boldsymbol{s}_i, \\ \boldsymbol{z}_{i-1} \cdot \boldsymbol{s}_i = -\boldsymbol{z}_i \cdot \boldsymbol{s}_i = \boldsymbol{z}_{i+1} \cdot \boldsymbol{s}_i, \end{aligned} \tag{33}$$

producing

$$(\boldsymbol{R}_{i+1} - \boldsymbol{R}_{i-1})^\mathsf{T} \boldsymbol{s}_i = \boldsymbol{0}. \tag{34}$$

From Eq. (34), without knowing $\boldsymbol{d}_{i-1}$, $\boldsymbol{d}_i$, and $\boldsymbol{d}_{i+1}$, the vector $\boldsymbol{s}_i$ can be calculated as

$$\begin{aligned} \begin{bmatrix} 0 & -s_z & s_y \\ s_z & 0 & -s_x \\ -s_y & s_x & 0 \end{bmatrix} &= \boldsymbol{R}_{i-1}^\mathsf{T} \boldsymbol{R}_{i+1} - \boldsymbol{R}_{i+1}^\mathsf{T} \boldsymbol{R}_{i-1}, \\ \boldsymbol{s}_i &= \boldsymbol{R}_{i-1} \left\{s_x, s_y, s_z\right\}^\mathsf{T}. \end{aligned} \tag{35}$$

The vector $\boldsymbol{s}_i$ serves not only as the normal vector to the plane formed by the three tips but also as the rotation axis between $\boldsymbol{R}_{i-1}$ and $\boldsymbol{R}_{i+1}$ in the fixed frame.

The reachability criterion for a two-segment continuum robot may now be explicitly stated. Let any two frames $\boldsymbol{R}_{i-1}$, $\boldsymbol{R}_{i+1}$, $\boldsymbol{d}_{i-1}$, and $\boldsymbol{d}_{i+1}$ be given. Satisfying Eq. (32) is sufficient to ensure the reachability of a two-segment continuum robot. Observe that this statement does not allow for $\boldsymbol{R}_{i+1}$ and $\boldsymbol{d}_{i+1}$ to be selected arbitrarily. The two-segment reachability criterion is consistent with the result from the literature that, even though there are six parameters associated with a two-segment continuum robot, the location of the second frame may not be arbitrarily selected. For the same $\boldsymbol{R}_{i+1}$, Eq. (32) indicates that all possible $\boldsymbol{d}_{i+1}$ form a tip plane.

B. Kinematic Redundancy of Two-Segment Continuum Robot

The end-effector of a two-segment continuum robot has been found to possess five-DoF through Jacobian rank calculations [26], [6]. However, since a two-segment continuum robot has six-DoF (three-DoF for each segment), indicating a one-DoF redundancy in the inverse kinematics problem. This section investigates the kinematic redundancy present in a two-segment continuum robot. This is achieved by analyzing the feasible positions of the middle tip, denoted as $\boldsymbol{d}_i$, using the position and orientations at the two ends of the robot, namely $\boldsymbol{R}_{i-1}$, $\boldsymbol{R}_{i+1}$, $\boldsymbol{d}_{i-1}$, and $\boldsymbol{d}_{i+1}$ such that the previous reachability condition is satisfied.

With $\boldsymbol{s}_i$ determined by the rotation axis between $\boldsymbol{R}_{i-1}$ and $\boldsymbol{R}_{i+1}$ from Eq. (35), the tip plane that includes $\boldsymbol{d}_i$ is now

IEEE Robotics and Automation Letters (RA-L) paper, presented at ICRA 2024, Yokohama, Japan. Cite as RA-L paper.

explicit. Note that $\boldsymbol{s}_i$ is in the bisecting planes of segments i and $i+1$ from Eq. (33). Due to the equality in Eq. (33), the angle between $\boldsymbol{z}_{i-1}$ and $\boldsymbol{s}_i$ and the angle between $\boldsymbol{z}_i$ and $\boldsymbol{s}_i$ are observed to be supplementary, making these vectors have equal angles to opposite sides of the tip plane. Thus, the set of all possible $\boldsymbol{z}_i$ forms a "cone" around the axis $\boldsymbol{s}_i$, with $\boldsymbol{z}_{i-1}$ located on the opposite side of the tip plane as shown in Fig. 2.

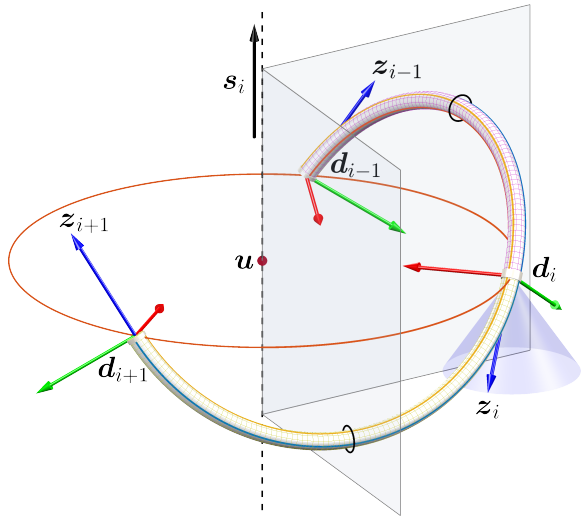

Fig. 2. The tip circle of a two-segment continuum robot is shown in red. The two bisecting planes and the tip plane intersect at the center of the circle $\boldsymbol{u}$ and $\boldsymbol{s}_i$ is normal to the tip plane. The cone through $\boldsymbol{d}_i$ shows all possible $\boldsymbol{z}_i$ that solve the inverse kinematics problem.

A specific solution for $\boldsymbol{z}_i$ can be identified by specifying a rotation angle $\eta \in [0, 2\pi)$,

$$\boldsymbol{z}_i = -\boldsymbol{R}(\boldsymbol{s}_i, \eta)\boldsymbol{z}_{i-1}, \tag{36}$$

where $\boldsymbol{R}(\boldsymbol{s}_i, \eta)$ is a rotation by η around the axis $\boldsymbol{s}_i$. Note that the vectors $\boldsymbol{x}_i$ and $\boldsymbol{y}_i$ remain unspecified at this time.

The corresponding $\boldsymbol{d}_i$ is now calculated. Considering the relationships in $\boldsymbol{z}$, Eq. (20) can be rewritten as

$$\begin{aligned} \boldsymbol{z}_{i-1} \cdot (\boldsymbol{d}_i - \boldsymbol{d}_{i-1}) &= \boldsymbol{z}_i \cdot (\boldsymbol{d}_i - \boldsymbol{d}_{i-1}), \\ \boldsymbol{z}_i \cdot (\boldsymbol{d}_{i+1} - \boldsymbol{d}_i) &= \boldsymbol{z}_{i+1} \cdot (\boldsymbol{d}_{i+1} - \boldsymbol{d}_i). \end{aligned} \tag{37}$$

Combining the definition of $\boldsymbol{s}_i$ with Eq. (37),

$$\boldsymbol{d}_i = \begin{bmatrix} \boldsymbol{s}_i^\mathsf{T} \\ (\boldsymbol{z}_i - \boldsymbol{z}_{i-1})^\mathsf{T} \\ (\boldsymbol{z}_{i+1} - \boldsymbol{z}_i)^\mathsf{T} \end{bmatrix}^{-1} \begin{Bmatrix} \boldsymbol{s}_i \cdot \boldsymbol{d}_{i-1} \\ (\boldsymbol{z}_i - \boldsymbol{z}_{i-1}) \cdot \boldsymbol{d}_{i-1} \\ (\boldsymbol{z}_{i+1} - \boldsymbol{z}_i) \cdot \boldsymbol{d}_{i+1} \end{Bmatrix}. \tag{38}$$

This computation capitalizes on the redundancy in a two-segment continuum robot by utilizing η, which serves to define the value of the middle tip $\boldsymbol{d}_i$. With the determination of $\boldsymbol{d}_i$, the value of $\boldsymbol{R}_i$ is uniquely determined from Eq. (31).

C. The Tip Circle

Assume no specific configuration for the two-segment continuum robot is yet identified. Three planes have been identified for this robot, the tip plane and the bisecting planes of segments i and $i+1$. The three planes intersect at a point, denoted $\boldsymbol{u}$. Note that $\boldsymbol{u}$ may be substituted for $\boldsymbol{p}$ in Eq. (13) for both segments i and $i+1$. From the definition of the normal vector $\boldsymbol{s}_i$ and the fact that the intersection point $\boldsymbol{u}$ lies on the tip plane,

$$(\boldsymbol{d}_i - \boldsymbol{u}) \cdot \boldsymbol{s}_i = 0. \tag{39}$$

From Eqs. (15), (18), and (19) and the fact that the intersection point $\boldsymbol{u}$ lies on both bisecting planes,

$$\begin{aligned} \boldsymbol{x}_{i-1} \cdot (\boldsymbol{u} - \boldsymbol{d}_{i-1}) &= \cdots = \boldsymbol{x}_{i+1} \cdot (\boldsymbol{u} - \boldsymbol{d}_{i+1}), \\ \boldsymbol{y}_{i-1} \cdot (\boldsymbol{u} - \boldsymbol{d}_{i-1}) &= \cdots = \boldsymbol{y}_{i+1} \cdot (\boldsymbol{u} - \boldsymbol{d}_{i+1}), \\ \boldsymbol{z}_{i-1} \cdot (\boldsymbol{u} - \boldsymbol{d}_{i-1}) &= \cdots = \boldsymbol{z}_{i+1} \cdot (\boldsymbol{u} - \boldsymbol{d}_{i+1}). \end{aligned} \tag{40}$$

Additionally, $\boldsymbol{u}$ is equidistant from $\boldsymbol{d}_{i-1}$, $\boldsymbol{d}_i$, and $\boldsymbol{d}_{i+1}$,

$$\|\boldsymbol{u} - \boldsymbol{d}_{i-1}\| = \|\boldsymbol{u} - \boldsymbol{d}_i\| = \|\boldsymbol{u} - \boldsymbol{d}_{i+1}\|. \tag{41}$$

Equations (39), (40), and (41) produce

$$\boldsymbol{u} = \begin{bmatrix} \boldsymbol{s}_i^\mathsf{T} \\ (\boldsymbol{z}_{i-1} - \boldsymbol{z}_{i+1})^\mathsf{T} \\ (\boldsymbol{d}_{i-1} - \boldsymbol{d}_{i+1})^\mathsf{T} \end{bmatrix}^{-1} \begin{Bmatrix} \boldsymbol{s}_i \cdot \boldsymbol{d}_{i-1} \\ \boldsymbol{z}_{i-1} \cdot \boldsymbol{d}_{i-1} - \boldsymbol{z}_{i+1} \cdot \boldsymbol{d}_{i+1} \\ \frac{1}{2}(\boldsymbol{d}_{i-1} \cdot \boldsymbol{d}_{i-1} - \boldsymbol{d}_{i+1} \cdot \boldsymbol{d}_{i+1}) \end{Bmatrix}. \tag{42}$$

Note that if the $\boldsymbol{z}$ instance of Eq. (42) is identically $\boldsymbol{0}$, the $\boldsymbol{x}$ or $\boldsymbol{y}$ equation is used instead. Examining Eq. (41), the set of all possible $\boldsymbol{d}_i$ are observed to lie on a *tip circle* centered about the intersection point $\boldsymbol{u}$ and in the tip plane. The identification of the tip circle of a two-segment continuum robot addresses the inverse kinematics problem.

The inverse kinematics problem in a two-segment continuum robot is now readily solved with knowledge of the base and end-effector position and orientations. The tip circle center $\boldsymbol{u}$ is calculated using Eq. (42). The tip circle's radius is determined as the distance between $\boldsymbol{u}$ and $\boldsymbol{d}_{i-1}$ or $\boldsymbol{d}_{i+1}$. A circle centered at $\boldsymbol{u}$ is constructed, perpendicular to vector $\boldsymbol{s}_i$, which is calculated using Eq. (35). Any point on this circle is selected as $\boldsymbol{d}_i$ to obtain a solution for the inverse kinematics problem. Once the positions for all tips are known, all configuration parameters are obtained using the method in the last paragraph of Sec. II. A video illustrates the kinematic redundancy [33].

V. Three-Segment Continuum Robot

A three-segment continuum robot has six-DoF at the end-effector. This is the minimum number of segments needed to arbitrarily place an end-effector frame. However, since a three-segment continuum robot has nine-DoF (three-DoF for each segment), indicating a three-DoF redundancy in the inverse kinematics problem. This section investigates the kinematic redundancy present in a three-segment continuum robot. This is achieved by analyzing the feasible positions of tips i and $i+1$, using the positions and orientations at the two ends of the robot, namely $\boldsymbol{R}_{i-1}$, $\boldsymbol{R}_{i+2}$, $\boldsymbol{d}_{i-1}$, and $\boldsymbol{d}_{i+2}$. The four tips of the continuum robot are assumed to not be coplanar, a degenerate case discussed in Sec. VI.

A. Kinematic Redundancy of Three-Segment Continuum Robot

To address the inverse kinematics problem of a three-segment continuum robot, the conversion of the three-DoF redundancy into a one-DoF redundancy problem is first conducted. This is achieved by arbitrarily specifying two parameters, θ_i and ϕ_i, in the configuration space. The next step

IEEE Robotics and Automation Letters (RA-L) paper, presented at ICRA 2024, Yokohama, Japan. Cite as RA-L paper.

involves calculating the corresponding positions of $\boldsymbol{d}_i$ and $\boldsymbol{d}_{i+1}$ to solve the inverse kinematics problem. From Eqs. (2) and (6), the orientation $\boldsymbol{R}_i$ is specified by $\boldsymbol{R}_{i-1}$, θ_i, and ϕ_i,

$$\boldsymbol{R}_i = \boldsymbol{R}_{i-1}\boldsymbol{Z}(\phi_i)\boldsymbol{Y}(\theta_i)\boldsymbol{Z}(-\phi_i). \tag{43}$$

From Eq. (12),

$$\boldsymbol{d}_i = \boldsymbol{d}_{i-1} + c_i\boldsymbol{R}_{i-1}\boldsymbol{e}_i^{i-1}. \tag{44}$$

where the chord length c_i is the only unknown. The value of $\boldsymbol{d}_i$ has to satisfy Eq. (32),

$$(\boldsymbol{d}_{i+2} - \boldsymbol{d}_i)\cdot\boldsymbol{s}_{i+1} = 0, \tag{45}$$

where the vector $\boldsymbol{s}_{i+1}$ can be calculated as the rotation axis between $\boldsymbol{R}_i$ and $\boldsymbol{R}_{i+2}$ in the fixed frame via a similar approach in Eq. (35). Substituting Eq. (44) into (45), the chord length c_i is calculated as

$$c_i = \frac{(\boldsymbol{d}_{i+2} - \boldsymbol{d}_{i-1})\cdot\boldsymbol{s}_{i+1}}{\boldsymbol{R}_{i-1}\boldsymbol{e}_i^{i-1}\cdot\boldsymbol{s}_{i+1}}. \tag{46}$$

The value of $\boldsymbol{d}_i$ is now calculated by substituting c_i into Eq. (44). The tip circle for all possible locations of $\boldsymbol{d}_{i+1}$ is now specified by Eq. (42). With the determination of $\boldsymbol{d}_{i+1}$, the value of $\boldsymbol{R}_{i+1}$ is uniquely determined from Eq. (31). Thus, the selection of three parameters, θ_i, ϕ_i, and then η to identify $\boldsymbol{d}_{i+1}$ on the tip circle, the above calculations identify a unique configuration for a three-segment continuum robot dependent on the three-DoF redundancy.

B. The Tip Sphere

Assume no configuration for the three-segment continuum robot is yet identified. This robot has three bisecting planes, one plane corresponding to each segment. The three bisecting planes intersect at the point $\boldsymbol{o}$. From Eqs. (15), (18), and (19) and the fact that the intersection point $\boldsymbol{o}$ lies on the all three bisecting planes,

$$\begin{aligned}
\boldsymbol{x}_{i-1}\cdot(\boldsymbol{o}-\boldsymbol{d}_{i-1}) &= \cdots = \boldsymbol{x}_{i+2}\cdot(\boldsymbol{o}-\boldsymbol{d}_{i+2}),\\
\boldsymbol{y}_{i-1}\cdot(\boldsymbol{o}-\boldsymbol{d}_{i-1}) &= \cdots = \boldsymbol{y}_{i+2}\cdot(\boldsymbol{o}-\boldsymbol{d}_{i+2}),\\
\boldsymbol{z}_{i-1}\cdot(\boldsymbol{o}-\boldsymbol{d}_{i-1}) &= \cdots = -\boldsymbol{z}_{i+2}\cdot(\boldsymbol{o}-\boldsymbol{d}_{i+2}),
\end{aligned} \tag{47}$$

producing

$$\boldsymbol{o} = \begin{bmatrix}(\boldsymbol{x}_{i-1}-\boldsymbol{x}_{i+2})^\intercal\\ (\boldsymbol{y}_{i-1}-\boldsymbol{y}_{i+2})^\intercal\\ (\boldsymbol{z}_{i-1}+\boldsymbol{z}_{i+2})^\intercal\end{bmatrix}^{-1}\begin{Bmatrix}\boldsymbol{x}_{i-1}\cdot\boldsymbol{d}_{i-1}-\boldsymbol{x}_{i+2}\cdot\boldsymbol{d}_{i+2}\\ \boldsymbol{y}_{i-1}\cdot\boldsymbol{d}_{i-1}-\boldsymbol{y}_{i+2}\cdot\boldsymbol{d}_{i+2}\\ \boldsymbol{z}_{i-1}\cdot\boldsymbol{d}_{i-1}+\boldsymbol{z}_{i+2}\cdot\boldsymbol{d}_{i+2}\end{Bmatrix}. \tag{48}$$

Since $\boldsymbol{o}$ is equidistant from $\boldsymbol{d}_{i-1}$, $\boldsymbol{d}_i$, $\boldsymbol{d}_{i+1}$, and $\boldsymbol{d}_{i+2}$, the set of all possible $\boldsymbol{d}_i$ and $\boldsymbol{d}_{i+1}$ must lie on a *tip sphere* centered about the intersection point $\boldsymbol{o}$ as shown in Fig. 3.

The inverse kinematics problem in a three-segment continuum robot is now readily solved with knowledge of the base and end-effector position and orientations. The tip sphere center $\boldsymbol{o}$ is calculated using Eq. (48). The tip sphere's radius is determined as the distance between $\boldsymbol{o}$ and $\boldsymbol{d}_{i-1}$ or $\boldsymbol{d}_{i+2}$. A sphere centered at $\boldsymbol{o}$ is constructed. Any point on this sphere is selected as one of the unknown tips, $\boldsymbol{d}_i$ or $\boldsymbol{d}_{i+1}$. The other tip is now reduced to a location on the tip circle obtained from Eq. (42). Once the positions for all tips are known, all configuration parameters are obtained using the method in the last paragraph of Sec. II. A video was produced to illustrate the kinematic redundancy [33].

An alternative method for identifying three-DoF redundancy involves selecting three configuration parameters, as in specifying the lengths of three segments in the inverse kinematics. Currently, closed-form solutions for this scenario are not available, necessitating the use of numerical methods for solutions. Another approach is to define the orientation of an intermediate tip, solving for both unknown intermediate tip positions. Due to the reachability criteria in Eqs. (22), (23), and (24), specifying an orientation equates to selecting a pair of bending and azimuth angles of a segment, representing two DoFs. The position of the chosen tip must lie along a line defined by Eq. (25). Note that, this line intersects with the tip sphere at two distinct points, effectively determining the position of the chosen tip. To determine the third DoF, the position of the other unknown intermediate tip on the relevant tip circle, derived from Eq. (42), is specified.

VI. Degenerate Cases

Degenerate cases for the solutions to the inverse kinematics problems of two- and three-segment continuum robots are now considered.

A. Two-Segment Continuum Robot

For a two-segment continuum robot, degenerate cases arise when the matrix in Eq. (42) is non-invertible. There are three cases that cause this condition. The first case occurs when $\boldsymbol{R}_{i-1} \neq \boldsymbol{R}_{i+1}$, $\boldsymbol{d}_{i-1} = \boldsymbol{d}_{i+1}$. Substituting $\boldsymbol{d}_{i-1} = \boldsymbol{d}_{i+1}$ into Eq. (38),

$$\boldsymbol{d}_i = \begin{bmatrix}\boldsymbol{s}_i^\intercal\\ (\boldsymbol{z}_i-\boldsymbol{z}_{i-1})^\intercal\\ (\boldsymbol{z}_{i+1}-\boldsymbol{z}_i)^\intercal\end{bmatrix}^{-1}\begin{bmatrix}\boldsymbol{s}_i^\intercal\\ (\boldsymbol{z}_i-\boldsymbol{z}_{i-1})^\intercal\\ (\boldsymbol{z}_{i+1}-\boldsymbol{z}_i)^\intercal\end{bmatrix}\boldsymbol{d}_{i-1}, \tag{49}$$

revealing that

$$\boldsymbol{d}_{i-1} = \boldsymbol{d}_i = \boldsymbol{d}_{i+1}, \tag{50}$$

and the tip circle collapses to a single point. Observe from Eq. (10) that $c_i = 0$ and L_i must be 0 as $\boldsymbol{R}_{i-1} \neq \boldsymbol{R}_{i+1}$ would violate the choice of $\theta_i = 2\pi$.

The second case occurs when $\boldsymbol{R}_{i-1} = \boldsymbol{R}_{i+1}$, $\boldsymbol{d}_{i-1} \neq \boldsymbol{d}_{i+1}$. From Eq. (34), $\boldsymbol{s}_i$ is observed to be arbitrary. From Eq. (31), the relationship between $\boldsymbol{R}_{i-1}$ and $\boldsymbol{R}_{i+1}$ is

$$\boldsymbol{R}_{i+1} = \left(\boldsymbol{I} - 2\boldsymbol{e}_{i+1}\boldsymbol{e}_{i+1}^T\right)\left(\boldsymbol{I} - 2\boldsymbol{e}_i\boldsymbol{e}_i^T\right)\boldsymbol{R}_{i-1}. \tag{51}$$

With $\boldsymbol{R}_{i-1} = \boldsymbol{R}_{i+1}$, this is true when

$$\boldsymbol{e}_i = \pm\boldsymbol{e}_{i+1}. \tag{52}$$

Since $\boldsymbol{d}_{i-1} \neq \boldsymbol{d}_{i+1}$, $\boldsymbol{d}_i$ has to lie on the line that intersects $\boldsymbol{d}_{i-1}$ and $\boldsymbol{d}_{i+1}$ to satisfy Eq. (52). This scenario corresponds to a straight configuration of the robot in which all three tips are collinear, ensuring the equality of the base and end-effector orientations. The end-effector's position can be selected arbitrarily. The orientation of the intermediate tip can be determined using Eq. (31).

IEEE Robotics and Automation Letters (RA-L) paper, presented at ICRA 2024, Yokohama, Japan. Cite as RA-L paper.

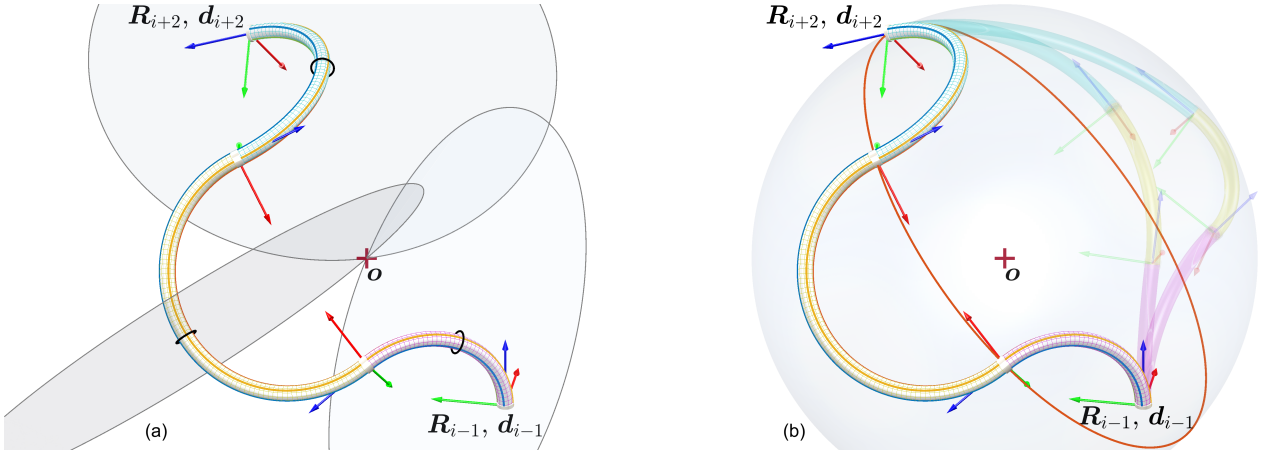

Fig. 3. (a) The three bisecting planes of a three-segment continuum robot intersect at the center of the tip sphere. (b) The tip sphere includes all possible locations of the tips of a three-segment continuum robot with given positions and orientations at both ends.

The final case occurs when $\boldsymbol{R}_{i-1} = \boldsymbol{R}_{i+1}$, $\boldsymbol{d}_{i-1} = \boldsymbol{d}_{i+1}$. The orientations being equal, Eqs. (51) and (52) apply. Since $\boldsymbol{d}_{i-1} = \boldsymbol{d}_{i+1}$,

$$-\boldsymbol{e}_i = \frac{\boldsymbol{d}_{i-1} - \boldsymbol{d}_i}{\|\boldsymbol{d}_{i-1} - \boldsymbol{d}_i\|} = \frac{\boldsymbol{d}_{i+1} - \boldsymbol{d}_i}{\|\boldsymbol{d}_{i+1} - \boldsymbol{d}_i\|} = \boldsymbol{e}_{i+1}, \tag{53}$$

satisfying Eq. (52) for any choice of $\boldsymbol{d}_i$. The resulting two-segment robot configuration is a circle comprised of the two segments.

B. Three-Segment Continuum Robot

For a three-segment continuum robot, two degenerate cases may arise. The first case occurs when $\boldsymbol{d}_{i-1} = \boldsymbol{d}_{i+2}$, and the matrix in Eq. (48) is invertible. Substituting $\boldsymbol{d}_{i-1} = \boldsymbol{d}_{i+2}$ into Eq. (48), results in

$$\boldsymbol{d}_{i-1} = \boldsymbol{d}_i = \boldsymbol{d}_{i+1} = \boldsymbol{d}_{i+2}, \tag{54}$$

and the tip sphere collapses to a single point. Observe from Eq. (10) that $c_i = 0$ and L_i must be 0 as $\boldsymbol{R}_{i-1} \neq \boldsymbol{R}_{i+2}$ would violate the choice of $\theta_i = 2\pi$.

The second case arises when the matrix in Eq. (48) is non-invertable, which occurs when $\boldsymbol{s}_i = \boldsymbol{s}_{i+1}$, and the two tip planes are the same because they must intersect $\boldsymbol{d}_i$ and $\boldsymbol{d}_{i+1}$. Thus, the four tips are coplanar. From $\boldsymbol{s}_i = \boldsymbol{s}_{i+1}$ and Eq. (33),

$$\begin{aligned} \boldsymbol{x}_{i-1} \cdot \boldsymbol{s}_i &= \cdots = \boldsymbol{x}_{i+2} \cdot \boldsymbol{s}_i, \\ \boldsymbol{y}_{i-1} \cdot \boldsymbol{s}_i &= \cdots = \boldsymbol{y}_{i+2} \cdot \boldsymbol{s}_i, \\ \boldsymbol{z}_{i-1} \cdot \boldsymbol{s}_i &= \cdots = -\boldsymbol{z}_{i+2} \cdot \boldsymbol{s}_i. \end{aligned} \tag{55}$$

Rotation matrices $\boldsymbol{R}_{i-1}$ and $\boldsymbol{R}_{i+2}$ that satisfy Eq. (55) have the property that

$$\boldsymbol{x}_{i-1} - \boldsymbol{x}_{i+2} \parallel \boldsymbol{y}_{i-1} - \boldsymbol{y}_{i+2} \parallel \boldsymbol{z}_{i-1} + \boldsymbol{z}_{i+2}. \tag{56}$$

Thus, the matrix in Eq. (48) is non-invertible and, further, has rank 1 as shown in Appendix.

The following process is used to define the plane for the degenerate tip sphere. First, find a vector $\boldsymbol{e}_i$ in the degenerate plane and specify the value of $\boldsymbol{R}_i$. If $\boldsymbol{d}_{i-1} \neq \boldsymbol{d}_{i+2}$, use Eq. (25) with the difference of $i-1$ and $i+2$, resulting in a vector $\boldsymbol{e}_i$ in the degenerate plane. Otherwise, if $\boldsymbol{d}_{i-1} = \boldsymbol{d}_{i+2}$, then $\boldsymbol{e}_i$ can be selected arbitrarily. Having $\boldsymbol{e}_i$, the corresponding $\boldsymbol{R}_i$ is obtained using Eq. (31). Second, determine the normal vector of the degenerate plane. If $\boldsymbol{R}_i \neq \boldsymbol{R}_{i+2}$, then $\boldsymbol{s}_{i+1}$ is determined from the rotation axis between $\boldsymbol{R}_i$ and $\boldsymbol{R}_{i+2}$ using Eq. (35). Otherwise, if $\boldsymbol{R}_i = \boldsymbol{R}_{i+2}$, then $\boldsymbol{s}_{i+1}$ is determined from the rotation axis between $\boldsymbol{R}_{i-1}$ and $\boldsymbol{R}_{i+2}$ using Eq. (35). Having $\boldsymbol{d}_{i-1}$, $\boldsymbol{d}_{i+2}$, and $\boldsymbol{s}_{i+1}$, the equation of the degenerate plane is readily determined. Any point in this plane may be selected as $\boldsymbol{d}_i$ and the corresponding $\boldsymbol{R}_i$ calculated using Eq. (31). The remaining tip, $\boldsymbol{d}_{i+1}$, sits on the tip circle that lies in this plane and passes through $\boldsymbol{d}_i$ and $\boldsymbol{d}_{i+2}$.

VII. Conclusion

This letter presents the kinematic analysis for general PCC continuum robots through three segments. The analysis starts by identifying the characteristics of a one-segment continuum robot. Utilizing these properties, reachability criteria are proposed that can be employed to determine if a given position and orientation are reachable by a one- or two-segment continuum robot. Using the criterion of a one-segment continuum robot, the calculation between neighboring orientations is simplified. Moreover, the investigation of the kinematic redundancy of two- and three-segment continuum robots reveals that the possible positions of the tips of a two- and three-segment continuum robot lie on the same circle and the same sphere, respectively. The closed-form solutions to the inverse kinematics problems of two- and three-segment continuum robots are provided and the degenerate cases are considered.

Appendix: Proof of Equation (56)

The following statements prove Eq. (56). With any two rotation matrices $\boldsymbol{R}_0$ and $\boldsymbol{R}_1$, there exists a rotation axis $\boldsymbol{s} \neq \boldsymbol{0}$ such that

$$\boldsymbol{R}_0^\intercal \boldsymbol{s} = \boldsymbol{R}_1^\intercal \boldsymbol{s}, \tag{57}$$

producing

$$(\boldsymbol{x}_0 - \boldsymbol{x}_1) \cdot \boldsymbol{s} = (\boldsymbol{y}_0 - \boldsymbol{y}_1) \cdot \boldsymbol{s} = (\boldsymbol{z}_0 - \boldsymbol{z}_1) \cdot \boldsymbol{s} = 0. \tag{58}$$

IEEE Robotics and Automation Letters (RA-L) paper, presented at ICRA 2024, Yokohama, Japan. Cite as RA-L paper.

Given that

$$\begin{vmatrix} (\boldsymbol{x}_0 - \boldsymbol{x}_1)^\intercal \\ (\boldsymbol{y}_0 - \boldsymbol{y}_1)^\intercal \\ (\boldsymbol{z}_0 + \boldsymbol{z}_1)^\intercal \end{vmatrix} = 0, \tag{59}$$

then,

$$\alpha(\boldsymbol{x}_0 - \boldsymbol{x}_1) + \beta(\boldsymbol{y}_0 - \boldsymbol{y}_1) = \boldsymbol{z}_0 + \boldsymbol{z}_1, \tag{60}$$

where α and β are constants. Taking the dot product of both sides of Eq. (60) with $\boldsymbol{s}$ and substituting the $\boldsymbol{x}$ and $\boldsymbol{y}$ instances of Eq. (58), produces

$$(\boldsymbol{z}_0 + \boldsymbol{z}_1) \cdot \boldsymbol{s} = 0. \tag{61}$$

From Eq. (61) and the $\boldsymbol{z}$ instance of Eq. (58), $\boldsymbol{s}$ is perpendicular to both $\boldsymbol{z}_0$ and $\boldsymbol{z}_1$, producing

$$\boldsymbol{s} = \alpha_0 \boldsymbol{x}_0 + \beta_0 \boldsymbol{y}_0 = \alpha_1 \boldsymbol{x}_1 + \beta_1 \boldsymbol{y}_1, \tag{62}$$

where α_0, α_1, β_0, and β_1 are constants. Substituting Eq. (62) into (57) produces $\alpha_0 = \alpha_1$ and $\beta_0 = \beta_1$,

$$\alpha_0(\boldsymbol{x}_0 - \boldsymbol{x}_1) + \beta_0(\boldsymbol{y}_0 - \boldsymbol{y}_1) = \boldsymbol{0}. \tag{63}$$

From Eqs. (60) and (63),

$$\boldsymbol{x}_0 - \boldsymbol{x}_1 \parallel \boldsymbol{y}_0 - \boldsymbol{y}_1 \parallel \boldsymbol{z}_0 + \boldsymbol{z}_1. \tag{64}$$

Thus, if the matrix in Eq. (59) is non-invertible, then Eq. (64) has to be satisfied.

REFERENCES

[1] R. J. Webster III and B. A. Jones, "Design and kinematic modeling of constant curvature continuum robots: A review," *The International Journal of Robotics Research*, vol. 29, no. 13, pp. 1661–1683, 2010.

[2] I. D. Walker, H. Choset, and G. S. Chirikjian, "Snake-like and continuum robots," *Springer Handbook of Robotics*, pp. 481–498, 2016.

[3] P. E. Dupont, N. Simaan, H. Choset, and C. Rucker, "Continuum robots for medical interventions," *Proceedings of the IEEE*, vol. 110, no. 7, pp. 847–870, 2022.

[4] M. Rolf and J. J. Steil, "Constant curvature continuum kinematics as fast approximate model for the bionic handling assistant," in *2012 IEEE/RSJ International Conference on Intelligent Robots and Systems*. IEEE, 2012, pp. 3440–3446.

[5] O. Fischer, Y. Toshimitsu, A. Kazemipour, and R. K. Katzschmann, "Dynamic task space control enables soft manipulators to perform real-world tasks," *Advanced Intelligent Systems*, vol. 5, no. 1, p. 2200024, 2023.

[6] A. Garriga-Casanovas and F. Rodriguez y Baena, "Kinematics of continuum robots with constant curvature bending and extension capabilities," *Journal of Mechanisms and Robotics*, vol. 11, no. 1, p. 011010, 2019.

[7] Y. Wang, Z. Wu, L. Wang, B. Feng, and K. Xu, "Inverse kinematics and dexterous workspace formulation for 2-segment continuum robots with inextensible segments," *IEEE Robotics and Automation Letters*, vol. 7, no. 1, pp. 510–517, 2021.

[8] M. Russo, S. M. H. Sadati, X. Dong, A. Mohammad, I. D. Walker, C. Bergeles, K. Xu, and D. A. Axinte, "Continuum robots: An overview," *Advanced Intelligent Systems*, vol. 5, no. 5, p. 2200367, 2023.

[9] G. S. Chirikjian and J. W. Burdick, "Hyper-redundant robot mechanisms and their applications," in *Proceedings IROS '91:IEEE/RSJ International Workshop on Intelligent Robots and Systems '91*, vol. 1. IEEE, 1991, pp. 185–190.

[10] D. C. Rucker, B. A. Jones, and R. J. Webster III, "A geometrically exact model for externally loaded concentric-tube continuum robots," *IEEE transactions on robotics*, vol. 26, no. 5, pp. 769–780, 2010.

[11] C. Della Santina and D. Rus, "Control oriented modeling of soft robots: the polynomial curvature case," *IEEE Robotics and Automation Letters*, vol. 5, no. 2, pp. 290–298, 2019.

[12] A. Shiva, S. H. Sadati, Y. Noh, J. Fraś, A. Ataka, H. Würdemann, H. Hauser, I. D. Walker, T. Nanayakkara, and K. Althoefer, "Elasticity versus hyperelasticity considerations in quasistatic modeling of a soft finger-like robotic appendage for real-time position and force estimation," *Soft Robotics*, vol. 6, no. 2, pp. 228–249, 2019.

[13] C. Armanini, F. Boyer, A. T. Mathew, C. Duriez, and F. Renda, "Soft robots modeling: A structured overview," *IEEE Transactions on Robotics*, 2023.

[14] X. Huang, J. Zou, and G. Gu, "Kinematic modeling and control of variable curvature soft continuum robots," *IEEE/ASME Transactions on Mechatronics*, vol. 26, no. 6, pp. 3175–3185, 2021.

[15] S. H. Sadati, S. E. Naghibi, A. Shiva, B. Michael, L. Renson, M. Howard, C. D. Rucker, K. Althoefer, T. Nanayakkara, S. Zschaler *et al.*, "Tmtdyn: A matlab package for modeling and control of hybrid rigid–continuum robots based on discretized lumped systems and reduced-order models," *The International Journal of Robotics Research*, vol. 40, no. 1, pp. 296–347, 2021.

[16] F. Renda, F. Boyer, J. Dias, and L. Seneviratne, "Discrete cosserat approach for multisection soft manipulator dynamics," *IEEE Transactions on Robotics*, vol. 34, no. 6, pp. 1518–1533, 2018.

[17] F. Renda, C. Armanini, V. Lebastard, F. Candelier, and F. Boyer, "A geometric variable-strain approach for static modeling of soft manipulators with tendon and fluidic actuation," *IEEE Robotics and Automation Letters*, vol. 5, no. 3, pp. 4006–4013, 2020.

[18] Y. Jin and H.-J. Su, "A compliant hinge joint driven by the pneunets bending actuator for enhancing the performance of soft robots," in *International Design Engineering Technical Conferences and Computers and Information in Engineering Conference*. American Society of Mechanical Engineers, 2023, p. 114816.

[19] E. Ripperger and G. Krishnan, "Design space enumerations for pneumatically actuated soft continuum manipulators," in *International Design Engineering Technical Conferences and Computers and Information in Engineering Conference*. American Society of Mechanical Engineers, 2023, p. 116930.

[20] Y. Toshimitsu, K. W. Wong, T. Buchner, and R. Katzschmann, "Sopra: Fabrication & dynamical modeling of a scalable soft continuum robotic arm with integrated proprioceptive sensing," in *2021 IEEE/RSJ International Conference on Intelligent Robots and Systems (IROS)*. IEEE, 2021, pp. 653–660.

[21] C. Della Santina, A. Bicchi, and D. Rus, "On an improved state parametrization for soft robots with piecewise constant curvature and its use in model based control," *IEEE Robotics and Automation Letters*, vol. 5, no. 2, pp. 1001–1008, 2020.

[22] S. Neppalli, M. A. Csencsits, B. A. Jones, and I. D. Walker, "Closed-form inverse kinematics for continuum manipulators," *Advanced Robotics*, vol. 23, no. 15, pp. 2077–2091, 2009.

[23] K. Xu and N. Simaan, "Analytic formulation for kinematics, statics, and shape restoration of multibackbone continuum robots via elliptic integrals," *Journal of Mechanisms and Robotics*, vol. 2, no. 1, p. 011006, 2010.

[24] B. Zhao, L. Zeng, B. Wu, and K. Xu, "A continuum manipulator with closed-form inverse kinematics and independently tunable stiffness," in *2020 IEEE International Conference on Robotics and Automation (ICRA)*. IEEE, 2020, pp. 1847–1853.

[25] C. Alessi, E. Falotico, and A. Lucantonio, "Ablation study of a dynamic model for a 3d-printed pneumatic soft robotic arm," *IEEE Access*, 2023.

[26] B. A. Jones and I. D. Walker, "Kinematics for multisection continuum robots," *IEEE Transactions on Robotics*, vol. 22, no. 1, pp. 43–55, 2006.

[27] P. Sears and P. E. Dupont, "Inverse kinematics of concentric tube steerable needles," in *Proceedings 2007 IEEE international conference on robotics and automation*. IEEE, 2007, pp. 1887–1892.

[28] B. A. Jones and I. D. Walker, "Practical kinematics for real-time implementation of continuum robots," *IEEE Transactions on Robotics*, vol. 22, no. 6, pp. 1087–1099, 2006.

[29] L. Jiajia, D. Fuxin, L. Yibin, L. Yanqiang, Z. Tao, and Z. Gang, "A novel inverse kinematics algorithm using the kepler oval for continuum robots," *Applied Mathematical Modelling*, vol. 93, pp. 206–225, 2021.

[30] G. S. Chirikjian and J. W. Burdick, "A modal approach to hyper-redundant manipulator kinematics," *IEEE Transactions on Robotics and Automation*, vol. 10, no. 3, pp. 343–354, 1994.

[31] F. Fahimi, H. Ashrafiuon, and C. Nataraj, "An improved inverse kinematic and velocity solution for spatial hyper-redundant robots," *IEEE Transactions on Robotics and Automation*, vol. 18, no. 1, pp. 103–107, 2002.

[32] Y. Li, A. P. Murray, and D. H. Myszka, "A backbone-driven approach for the positioning of continuum robots," in *International Design Engineering Technical Conferences and Computers and Information in Engineering Conference*. American Society of Mechanical Engineers, 2023, p. 114773.

[33] Y. Li. (2023) Redundancy in two- and three-segment PCC continuum robots. YouTube. [Online]. Available: https://youtu.be/RiB1JVakjBM